

Laminar burning velocity measurements in constant volume vessels – reconciliation of flame front imaging and pressure rise methods

Nathan Hinton and Richard Stone¹, University of Oxford
Roger Cracknell, Shell Global Solutions

¹Corresponding Author Richard.stone@eng.ox.ac.uk

Highlights

- Direct comparisons between laminar burning velocity measurements made by flame front imaging and pressure rise methods.
- Correlations for the laminar burning velocity of methane/air mixtures.
- Correlations for the laminar burning velocity of biogas (60% methane, 40% carbon dioxide)/air mixtures.
- Correlations for the laminar burning velocity of ethanol/air mixtures.

Abstract

Laminar burning velocity measurements have been made in a constant volume vessel using both flame front imaging and the pressure rise methods. Results from the two different methods are shown to be the same, so long as appropriate techniques are used for analysing the data. Comparisons are presented for the laminar burning velocity of mixtures with air of methane, ethanol and biogas (60% methane, 40% carbon dioxide) for a wide range of flammable mixtures at pressures of 2 and 4 bar and temperatures of 380 and 450 K.

Methods for measuring the laminar burning velocity are still the subject of controversy, with different researchers favouring different approaches. Open flame techniques are very popular and the so-called heat flux method is now well established. The alternative technique of using a constant volume combustion vessel is also in common use, and has two distinct methods of use: either the imaging of flame front propagation at conditions of constant pressure, or the measurement of the pressure rise combined with a constant volume combustion model. The pressure rise method requires a more complex analysis, but has the advantage that a single experiment generates data across a range of linked temperatures and pressures, and the pressure and temperature rise also mean that data can be obtained for engine-like conditions.

Keywords

Laminar burning velocity; flame speed measurement; pressure rise measurement; methane; ethanol; biogas

1 Introduction

In the transport sector, biofuels such as blends including ethanol are becoming increasingly common as a way of reducing the greenhouse gas intensity of fuels, in conjunction with developments in engine technology that provide large gains in fuel efficiency. To fully realise these benefits,

fundamental combustion performance of new fuels needs to be well understood, both to evaluate the potential performance of the fuel, but also to provide input parameters for models used in technological development.

The laminar burning velocity is a fundamental property of a propagating premixed fuel-air flame that is dependent upon the mixture temperature, pressure, equivalence ratio and presence of inert components. It is defined as the speed of propagation of an unstretched, adiabatic, one-dimensional flame relative to the unburned gas into which it is propagating. Flame speed is when the mixture ahead of the flame front is not stationary, for example, when the burned gas behind the flame front is contained, so that the reduction in density of the burned gas and its increased volume displaces the mixture into which the flame is propagating. Values of laminar burning velocity are required for the validation of both full and reduced kinetic mechanisms, and as an input to turbulent combustion and engine models. For many applications such as modelling of combustion in engines, data is required for a wide range of temperatures and pressures, as well as a variety of equivalence ratios and diluent fractions, making burning velocity correlations a particularly convenient method of implementation [1].

A number of techniques have historically been used to determine the laminar burning velocities of fuel-air mixtures, and are described more fully in section 2. Those using constant volume combustion vessels are in common use, and broadly offer two distinct methods of determining burning velocities: imaging of the flame front propagation at conditions of constant pressure, or measurement of the pressure rise combined with a constant volume combustion model. Whilst these two techniques exist, researchers tend to prefer one technique or the other, or in some cases where optical access is not possible, are limited to a single method. No studies have been found which show direct comparisons of the results from these two methods to agree, in part due to the fact that results from the two techniques in a single experiment will relate to different conditions of temperature and pressure, or due to the fact that only one method is employed. Given that there are advantages to each method, the current work aims to reconcile results from the two techniques to demonstrate each as a viable method, thereby extending the potential range of data obtainable. Many studies are published that use the constant pressure data (see for example some recent papers [2, 3, 4]), yet these experiments could also have generated measurements for higher pressures and temperatures when a spherical vessel is used.

2 Background to Measurements of laminar burning velocities

Measurements of laminar burning velocities have historically been made using a variety of techniques, broadly divided into the categories of stationary and non-stationary flame methods. Stationary flame methods will typically use a burner into which a continuous mixture of fuel and oxidant is fed at a constant velocity. The stationary flame is then established at the mouth of the burner, from which measurements can be made. Simple burner techniques establish a conical flame, although problems exist regarding identification of the exact position of the flame front, heat losses to the burner rim, and the effect of flame shape on determined burning velocity [5]. More advanced flat flame burners are considered to provide more reliable results, and in particular the Heat Flux Burner [6] is increasingly used by many groups to establish highly accurate values of burning velocity. Another approach is to use a diverging channel, and a recent example of this is provided by Katoch *et al.* [7]. Whilst such methods are being developed to provide higher pressure measurements [8], limitations remain on the pressure at which data can be obtained. Non-stationary flame techniques are predominantly propagating spherical flames, either at conditions of constant

pressure or constant volume. The following review summarises the key steps in technique development and identifies the precautions and procedures that are needed for accurate measurements, namely: the exclusion of data affected by cellularity, appropriate corrections for the effects of stretch, use of a comprehensive calculation of the state of the burned and unburned gases, and choice of an appropriate equation when experimental data are being correlated.

Experiments involving constant volume combustion vessels date back to the work of Hopkinson [9], who measured the pressure rise during combustion. Hopkinson also identified the temperature gradient in the burned gas (about 500 K), though only recently has the pressure rise method taken account of the temperature gradient in the burned gas. Early examples of constant pressure flame speed measurements include the soap bubble method used by Stevens [10], in which a flammable mixture was ignited within a boundary which was free to move, preventing compression of the unburned gas ahead of the flame front as the flame propagates ahead of the expanding burned gas. By maintaining constant pressure, the flame speed can be evaluated using photography of the flame front. However, control of the initial conditions with this method is difficult and the range of fuels that can be tested is limited. Constant volume combustion bombs with rigid walls therefore became preferred and have been used extensively. Due to the fact that the initial stages of constant volume combustion take place at conditions of effectively constant pressure, flame front imaging at constant pressure, and measurement of the pressure rise as the flame propagates further, can both be used to determine the burning velocity. Knowing the density ratio between the unburned and burned gas enables the flame speed to be converted to the laminar burning velocity.

Fiock *et al.* [11] pioneered the use of imaging of flame fronts within a solid spherical vessel by means of a thin cylindrical glass ring mounted between the two halves of the vessel. However, their analysis combined the radius measured by imaging of the flame front with measurements of pressure rise and a model of constant volume combustion to determine the burning velocity (based upon consideration of the change of volume of a shell of unburned gas of small thickness) and so is therefore considered as a pressure rise measurement with imaging needed only to determine the flame radius as the pressure rises, rather than for constant pressure analysis. Subsequent developments of the constant volume vessel technique used the pressure rise to calculate the flame front position.

Lewis and von Elbe [12] were first to derive burning velocities from pressure measurements alone, by using a linear assumption between mass fraction burned and pressure rise, so as to estimate the radius of the flame during combustion. Metghalchi and Keck [13] developed a subsequent model based on the mass burning rate, and introduced a two zone numerical model in which the gas in the vessel is divided into burned and unburned gas zones separated by a thin flame front, and the equations of conservation of energy and volume are solved numerically. However, a limitation of using just two zones is that recompression of the burned gas is ignored. This recompression leads to a temperature gradient within the burned gas (as identified by Hopkinson) which cannot be modelled by just two zones. It has been shown by Stone *et al.* [14] that the difference between the linear mass fraction burned assumption of Lewis and von Elbe [12] and the results of the two zone model of Metghalchi and Keck [13] are not significant for the methane-air mixtures tested.

A number of studies attempted to include the effect of including the burned gas temperature gradient such as that of Bradley and Mitcheson [15]. Hill and Hung [16] and Elia *et al.* [17] both extended the analysis of Metghalchi and Keck [13] to include multiple shells within the burned gas region, to enable the temperature gradient within the burned gas to be modelled more accurately. The gases in each shell are assumed to be in chemical equilibrium, with the burned gas states calculated using the STANJAN solver [18] and thermodynamic properties of all gases calculated from JANAF tables

[19]. However, as summarised by Saeed and Stone [20], agreement between these models is generally poor, prompting development of a more rigorous multizone computational model. In this model, the mass inside the vessel is initially divided into a number of zones, which can be of either equal radius or equal mass. Each zone is then divided further into a number of elemental shells. The total number of elemental shells in the vessel corresponds to the number of time-steps chosen in the simulation, with flame front propagation seen as the consecutive consumption of the elemental shells. The equations of conservation of volume and internal energy are solved as first order differential equations of the pressure and unburned gas temperature in the vessel. The formulation is based upon the approach of Ferguson [21], with a program derived from the multi-zone spark ignition engine simulation program of Raine *et al.* [22]. This model then allowed the determination of burning velocities from the pressure record over the range of pressures and temperatures encountered during combustion; differences in burning velocity of up to 10% occurred when comparing the burning velocity values derived from the multi-zone model with the Lewis and von Elbe assumption of mass fraction burned being proportional to the pressure rise [12].

Advantages of the constant volume vessel technique include the ability to obtain data over an increased range of temperatures and pressures, as well as the ability to obtain a large number of data points from a single experiment. It is also possible to retain some of the residuals from a previous experiment, thereby eliminating approximations with ‘synthetic residuals’ [23]. These advantages led Rallis and Garforth [5] to describe the constant volume technique as “the most versatile and accurate” of the propagating flame methods. The ability to obtain such quantities of data also lends itself well to the fitting of burning velocity correlations. However, there are commonly objections to the technique, because the effects of flame stretch are ignored, and that without optical access, it becomes difficult to determine the onset of any flame front instabilities, (which violates the assumption of a smooth flame front and invalidates calculations of the burning velocity).

The concept of flame stretch was first introduced by Karlovitz [24], and has been well documented since. The effects of stretch on flame speed is first acknowledged by Palm-Leis and Strehlow [25]. It can be considered that the effects of stretch consist of curvature of the flame front, and straining of the flame front as it propagates, and is expressed as:

$$\alpha = \frac{1}{A} \frac{dA}{dt} \quad (1)$$

which in the case of a spherically expanding flame becomes:

$$\alpha = \frac{2}{r_f} \frac{dr_f}{dt} \quad (2)$$

Bradley *et al.* [26] attribute the large spread in burning velocity data in part due to insufficient attention being paid to the effects of stretch. Andrews and Bradley [27] claimed that beyond a flame radius of 50 mm the effects of stretch are negligible, and this would be satisfied by most measurements during the pressure rise phase of combustion, but obviously not during the constant pressure phase. However, with more accurate quantification of the stretch rates required to enable sufficiently accurate values of burning velocity to be obtained, the assumption of negligible effects of stretch in the pressure rise method may need to be reconsidered. This is particularly true of combustion in small vessels, where the pressure rise will begin at smaller radii for which the stretch rates are very high. Chen *et al.* [28] investigated the effects of stretch in constant volume vessels and present a stretch corrected flame speed (SCFS). Using a linear relationship between stretched burning velocity S_n and unstretched burning velocity S_u , via the unburned gas Markstein length, L_u :

$$S_n = -L_u \alpha + S_u \quad (3)$$

and noting the zeroth order between the stretched and unstretched burning velocities, they derived an expression to determine the effect of stretch rates on burning velocities derived from the pressure rise method. Their study considered an extreme case with a vessel radius of 60 mm and a Lewis number of 2.0 such that the stretch rates would be high and the effects of stretch more significant than unity Lewis numbers, and found that when the pressure increase was below 20%, the stretch effect on burning velocity was greater than 10%. This would then require corrections to the burning velocity by using values of unburned Markstein length as given in equation (3), obtained from constant pressure measurements or counterflow experiments. Marshall *et al.* [23] investigated the possibility of including a stretch correction term in the correlation, but this proved difficult since the Markstein length will be a function of equivalence ratio [29], pressure, and to a lesser extent temperature [26], and so the assumption of negligible effects of stretch was assumed. Elia *et al.* [13] showed that for a small stoichiometric methane-air flame, the biggest correction for stretch was only 1.0 cm/s, which reduced to 0.2 cm/s by the time the flame reached the edge of the vessel.

Some typical experimental data will help to put this discussion into context using data and computed values from the pressure rise data. Figure 1 shows how the pressure has barely risen by about 10% from the initial pressure of 4 bar by a flame radius of 35 mm, and how the high density ratio between the burned and unburned gas leads to a high flame speed. The flame speed reduces (relative to the burning velocity) with radius for three reasons:

1. The pressure rise increases the density of the burned gas, so tending to reduce the volume of the burned gas,
2. the volume of burned gas is proportional to radius cubed, so as the radius increases the incremental displacement of the flame for a given mass burned increment reduces,
3. as the radius increases the pressure rises so the unburned gas temperature rises and the density ratio will fall so the flame speed reduces.

Inspection of Eq. 2 shows that the effect of the larger radius and reduced flame speed both contribute to the substantial reduction in stretch rate as the pressure rises; at a radius of 35 mm the stretch rate is about 30 s^{-1} , and it will be seen later (Fig. 4d) that this is a very low stretch rate. Figure 2 shows how the burning velocity increases with radius for the same data as in Fig. 1. Although the pressure is rising substantially, this has a weaker effect on reducing the burning velocity compared with the rise in unburned gas temperature (from 380 K to over 600 K) that increases the burning velocity.

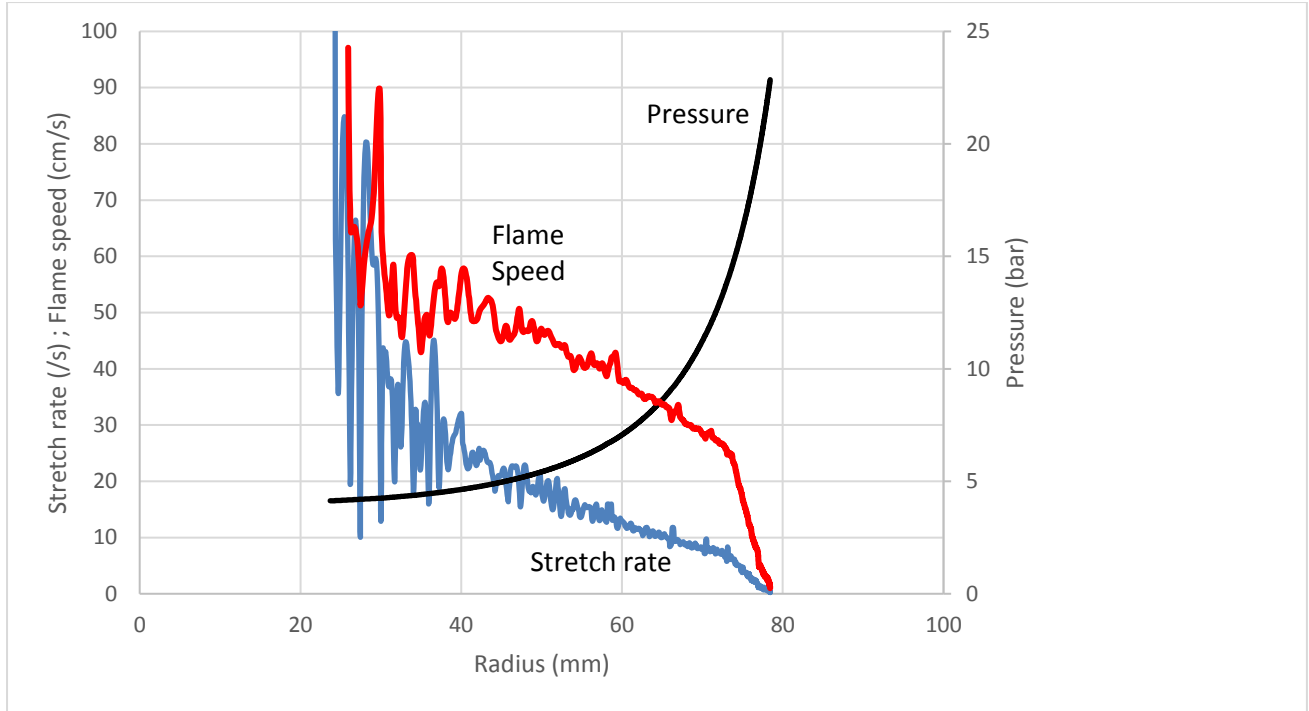


Figure 1 - The reduction in stretch rate as the flame radius increases and the flame speed, computed from the pressure rise data, reduces (methane equivalence ratio 1.4, initial pressure 4 bar and temperature 380 K)

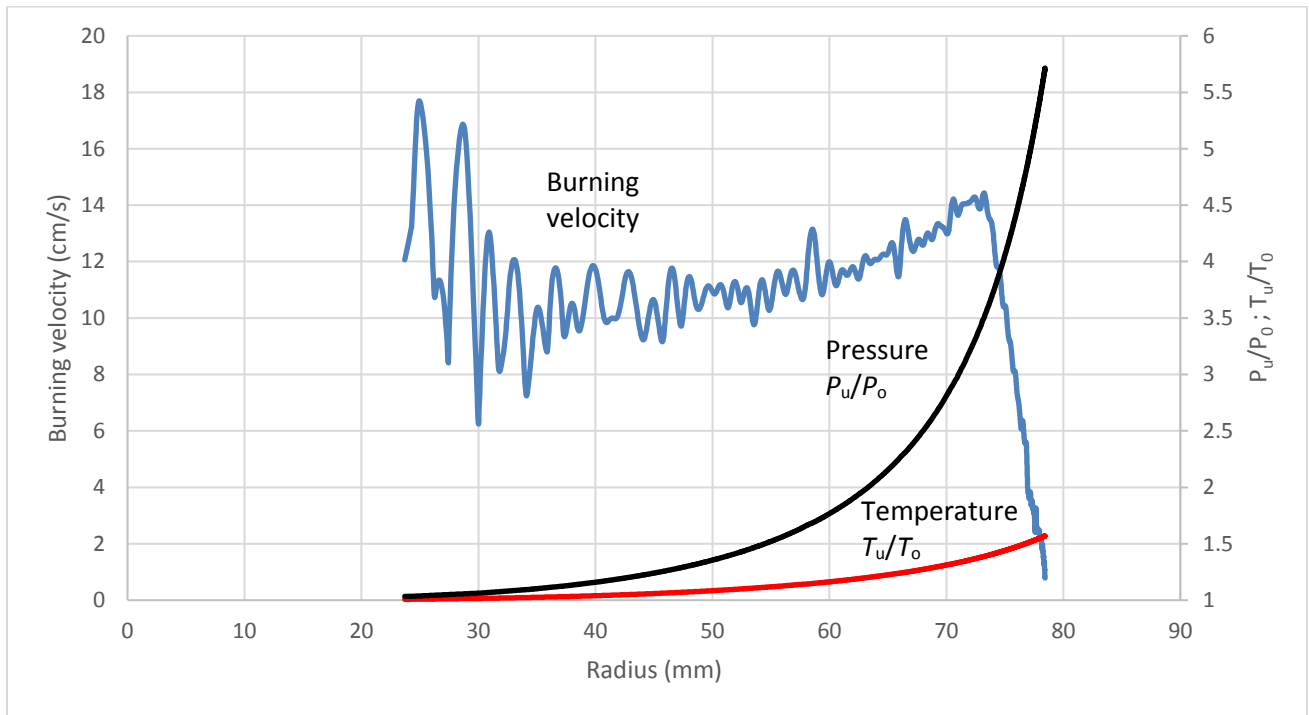


Figure 2 - The increase in burning velocity as the flame radius increases (methane equivalence ratio 1.4, initial pressure 1 bar and temperature 380 K)

With regards to the effect of cellularity, the presence of such instabilities in flames was demonstrated by Markstein [30] using propane flames burning in tubes; in the case of spherical expanding flames, spontaneous cell formation was shown by Manton *et al.* [31]. The hydrodynamic and thermo-acoustic causes of the instabilities in closed vessels that can distort the smooth spherical flame front are well summarised by Al-Shahrany *et al.* [32]. When these instabilities develop, a sharp increase in

flame speed is seen as a result of the increased flame front area. Since the constant volume combustion models used are based upon a smooth spherical flame front, this will lead to an incorrect calculation of the burning velocity. However, in some earlier constant volume experiments this effect might not have been considered.

As mentioned previously, burning velocities can also be obtained from flame front imaging alone, provided the imaging is limited to conditions of approximately constant pressure. This technique has gained much attention recently, as it allows the effects of ignition and flame stretch to be determined in a way not possible without optical access. The effects of stretch, by determining Markstein lengths, are as important to determine as the burning velocity measurements themselves if modelling is to be used of turbulent combustion. Typically schlieren photography is used for imaging of the flame front, as it is considered to give the best representation of the flame front position [5]. Bradley *et al.* relate the schlieren radius to the cold front radius in their computational study [33]. This schlieren radius is used to determine the flame speed as the rate of change of flame radius. Due to the small flame radii during the initial stages of propagation at constant pressure, the rates of flame stretch are large. Dowdy *et al.* [34] used a linear relationship between flame speed and stretch rate to define a Markstein length, which is independent of whether the stretch is due to curvature or strain. This allows an extrapolation to conditions of zero stretch and determination of an unstretched flame speed. Multiplication by the density ratio of burned and unburned gases then yields the laminar burning velocity at those conditions of temperature and pressure.

The effects of stretch upon flame speed, and therefore the method of extrapolation to obtain unstretched flame speeds, has received much attention in recent studies. Kelley and Law [35] suggest a non-linear relation, which has subsequently been reviewed. Chen [36] used a modelling study to compare the extrapolation methods and found that there was discrepancy as the Lewis number deviates from unity. Tahtouh *et al.* [37] and Halter *et al.* [38] also investigated the effects of extrapolation techniques upon the determined burning velocities and burned gas Markstein lengths, and noted that the inaccuracy introduced by the linear extrapolation can be reduced with a methodical reduction in the number of data points included in the extrapolation, although naturally reducing the number of points will make obtaining a reliable fit more difficult. Linear extrapolation is still widely used, e.g. [39], and a recent paper by Xiouris *et al.* [40] uses numerical modelling to justify a linear relation between the stretch rate and burning velocity. A novel technique has been developed by Varea *et al.* [41] to measure the burning velocity directly from the definition of the flame speed relative to the unburned gas ahead of the flame front. Techniques involving the imaging of flame front propagation at constant pressure are therefore popular, as they enable detailed study of the propagation, and the effects of stretch can be more precisely determined and accounted for when making measurements of burning velocity.

Few studies using constant volume combustion vessels have utilised both the flame front imaging and pressure rise techniques. Groff [42] conducted a study of propane-air flames in a constant volume combustion vessel and used imaging techniques to obtain flame speeds when the pressure rise was too small for pressure measurements, and measured the pressure rise along with a two zone model to determine burning velocities subsequently. Comparison of the two methods was, however, not possible since the conditions for which burning velocities were being determined were not equivalent. Furthermore, the values of burning velocity obtained from the flame front images were found by multiplying the flame speed directly by the density ratio, although it was subsequently shown [26] that this will result in incorrect values unless an unstretched value of flame speed has been used, and in this work no extrapolations to zero stretch have been performed. Farrell *et al.* [43] used both methods to determine burning velocities from a wide range of fuels at elevated temperatures and pressures, and found that the results from pressure measurements were

systematically higher than those from the flame front imaging method. It was suggested that this could be due to the fact that the pressure measurement records the evolution of the burned gas rather than the propagation of the flame front into the unburned gas [26], or that their method for extrapolating burning velocity measurements to the initial conditions contained some systematic error. A recent study that includes measurements from both techniques (Xiouris *et al.* [40]) has made indirect comparisons between the two techniques by means of modelling, but the experiments used different vessels. Therefore, a study to reconcile the two methods and make direct comparisons is of interest.

As explained previously, an often cited advantage of the pressure rise method is the wide range of data collected, which can be fitted to a correlation for use directly in combustion models and engine simulations. For example, the work of Lindström *et al.* [44] demonstrated how, incorporating a burning velocity correlation into an engine system dramatically reduced the number of input variables required. An appropriate consideration, therefore, is to compare the results of flame front image analysis with the correlations produced using the pressure rise method. Correlations found elsewhere in the literature are commonly based upon a polynomial function of equivalence ratio, multiplied by power law functions of temperature and pressure. Early versions of such correlations [13] give a second order polynomial of equivalence ratio and constant values of pressure and temperature exponents. Higher order polynomials have been used to represent effect of equivalence ratios, up to fourth order, e.g. Stone *et al.* [14]. In their subsequent work, Metghalchi and Keck [45] introduced a linear dependence of the pressure and temperature exponents upon equivalence ratio. The effect of temperature upon burning velocities has been identified as being of particular importance with regard to a number of issues, including to a certain extent preignition in spark ignition engines [46]. A study on the temperature dependence of ethanol-air flames by Konnov *et al.* [47] has shown a second order function of equivalence ratio as exponent on the temperature term in a simple power law relationship. Self-dependence of the temperature exponent on temperature was suggested by Marshall *et al.* [48], but was not found to be significant.

3 Experimental Setup, Procedure and Sources of Error

Figure 3 shows the experimental setup used in this work: it is a constant volume combustion bomb rig based upon that is described in [23] and [48]. The spherical vessel is constructed from stainless steel with a diameter of 160 mm, with one pair of windows (40 mm usable diameter) along an optical axis to allow imaging of the flame front. The vessel is rated to pressures up to 3.4 MPa. The combustion vessel is enclosed within a temperature controlled fan oven capable of raising the initial temperature to 450 K.

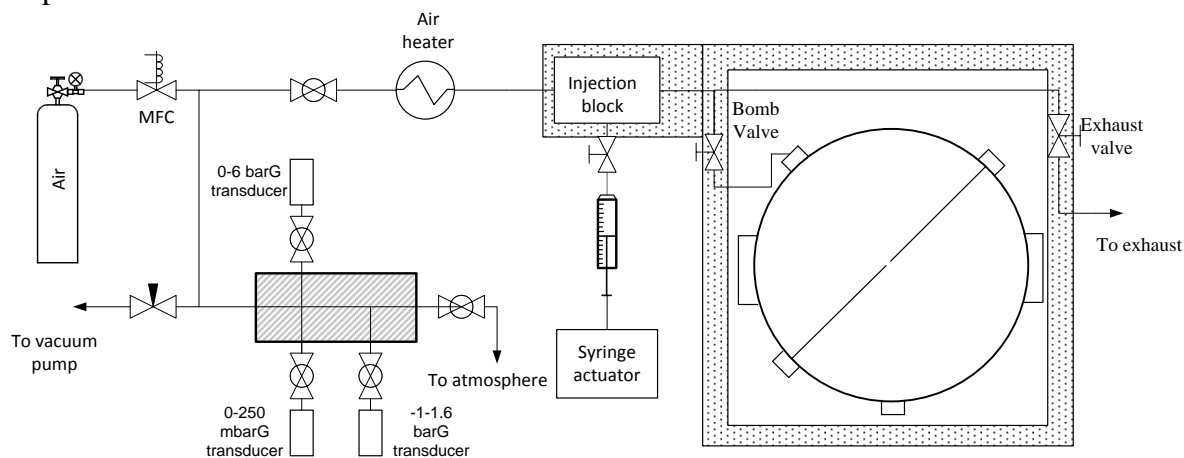


Figure 3 – Schematic diagram of the liquid fuel mixture preparation system

Mixtures are prepared using a method based upon Dalton's law of partial pressures. For gaseous fuels, fuel, air and diluent are added in stages, according to the calculated partial pressures required for each component. Three Druck PMP1400 piezo-resistive pressure transducers were used to monitor the pressure during preparation and covered the entire pressure range during mixture preparation. The temperature of the gas in the vessel was measured by an exposed junction K-type thermocouple, and the respective concentrations of fuel, air and diluent are calculated by the mixture preparation program implemented in LabVIEW. The liquid fuel mixture preparation system is shown schematically in Fig. 3. An air stream flowing at a rate controlled by a Mass Flow Controller (MFC) is heated before reaching the injection block to aid with evaporation of the injected fuel. The volume of fuel to produce a desired mixture at a given pressure and temperature is calculated by the LabVIEW program, and is injected into the heated air stream using a syringe and actuator. The rate of injection is chosen to ensure constant injection duration across all experiments, with the vessel pressure being kept below atmospheric pressure during injection. The mass of the syringe and injector are measured before and after injection, so that the correct final pressure of the mixture can be determined. The target final pressure is always above the experiment initial pressure, so that mixture can be removed to obtain the correct initial pressure. The injection block itself is heated to around 90°C to assist with ensuring complete vaporisation of the fuel as it leaves the needle, and the co-flow of heated air ensures complete entrainment into the vessel. The block and short length of pipework to the temperature controlled oven are insulated to maintain the temperature of the inlet flow.

A pair of electrodes forms the spark gap at the centre of the vessel, with ignition driven by a conventional automotive inductive ignition system. Combustion pressure is measured by a Kistler 701A piezo-electric pressure transducer with a charge amplifier integrated with a LabVIEW based data acquisition system, and a sampling rate of 10 kHz. A folded pin-hole schlieren system is used to obtain flame front images, recorded using a Photron 1024 PCI high speed camera with 512x512 pixel resolution and a frame rate of 3000 fps [49, 50].

For a given fuel under test, a range of mixture equivalence ratios at different conditions of temperature and pressure are tested. During combustion the isentropic compression of the unburned gas leads to a linked temperature and pressure rise, so different initial temperatures and pressures can decouple the influence of temperature and pressure. The pressures that have typically been used are 1, 2 and 4 bar, with initial temperatures of 298, 380 and 450 K, to test a range of mixtures with equivalence ratios both lean and rich of stoichiometric.

4 Data analysis

A number of assumptions are required to justify the equations for determination of burning velocity and the combustion model used. The following summary of the key requirements and assumptions is derived from Luijten and de Goey [51]:

1. The unburned mixture is initially at rest.
2. Pressure and temperature of the gas are initially uniform.
3. Pressure remains uniform during combustion.
4. Total mass and volume of gas in the vessel is conserved.
5. Central ignition with negligible heat input (relevant to the constant pressure flame speed measurement).
6. The process is adiabatic (more relevant to the pressure rise measurement).
7. The effect of buoyancy is negligible.
8. The flame front is spherical and smooth.
9. The flame front is thin.

10. Effects of flame stretch are negligible for large flame radii.

11. The unburned gas is compressed isentropically (only relevant to the pressure rise measurement method data).

The assumption that the flame front is thin (namely of zero thickness), is an assumption that has more impact on the constant pressure technique than the pressure rise measurement technique, as the flame thickness can be expected to reduce as the pressure rises. Rallis and Garforth [5] indicate that flame thickness is of order 1 mm at ambient conditions; they also comment that there are uncertainties in defining the flame thickness and this confounds attempts at correcting for the flame thickness.

4.1 Flame front imaging method

The data analysis from a single experiment follows two paths, one for image analysis and a second for pressure rise analysis. The procedure is summarised in Fig. 4, with the right hand side of the diagram representing the flame front imaging analysis.

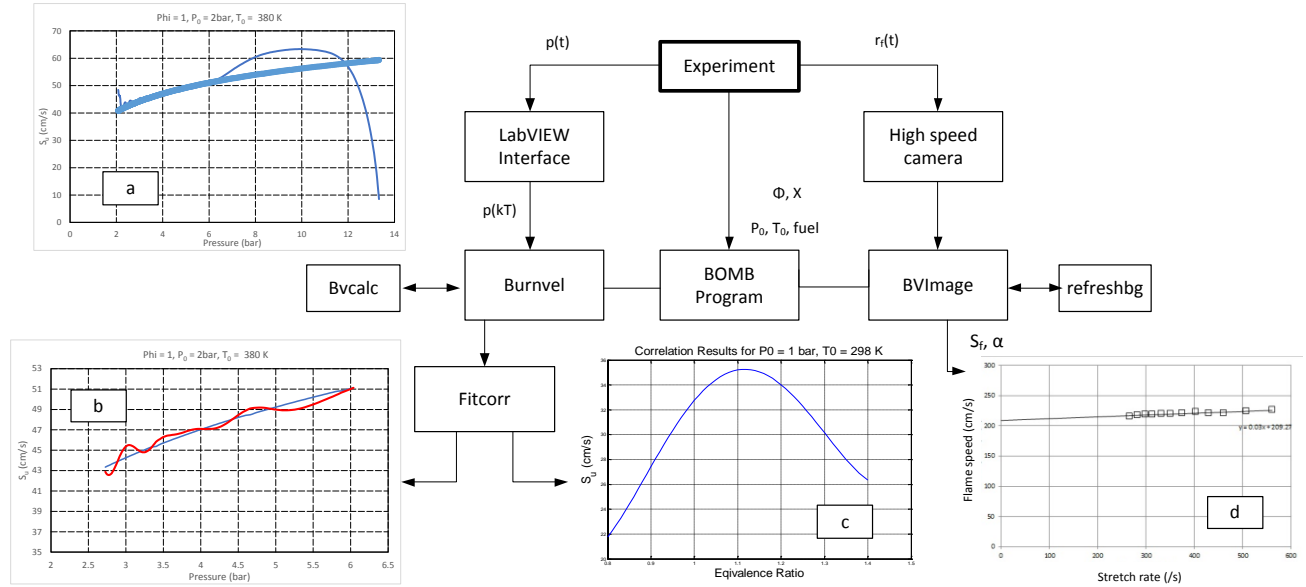


Figure 4 – Schematic diagram of data analysis procedures for both techniques, with insets that show (a) burning velocity calculated as the pressure rises, (b) fit of the global correlation to the data selected from a single experiment, (c) a sample plot from the resulting correlation and (d) extrapolation of flame speed to zero stretch from the flame imaging.

During the initial flame propagation following ignition, the flame is considered to propagate spherically outwards at conditions of constant pressure. The flame speed can be considered as the rate of change of flame radius:

$$S_f = \frac{dr_f}{dt} \quad (4)$$

where the flame radius is detected using schlieren images. The flame front appears on the schlieren image as a dark circle, and the radius is detected using an algorithm described by Marshall [50], which is contained within the BVImage routine. The schlieren radius is related to the flame radius as defined by Bradley et al. [26], and as a result of the high levels of curvature of the flame front in the initial stages of propagation, stretch rates will be high.

394 To obtain the unstretched flame speed S_s , a linear extrapolation of flame speed S_f against stretch rate
 395 is performed (Fig. 4d), with the gradient yielding the burned gas Markstein length L_b :

$$S_f = -L_b \alpha + S_s \quad (5)$$

396 The unstretched burning velocity can then be obtained by multiplying the unstretched flame speed by
 397 the density ratio of the burned and unburned gas, as calculated by the multizone combustion model
 398 of Saeed and Stone [20]. Hence, each experiment will yield a single value of burning velocity and
 399 burned gas Markstein length.

400

401 The BVImage routine also contains a cellularity detection algorithm, based upon edge detection
 402 methods on the basis that cellular instabilities are associated with the flame front dividing up into
 403 sub-dividing cells, which will be visible on the schlieren images as an increased number of distinct
 404 edges. When cellularity is detected, further data must not be included in either the flame front
 405 imaging or pressure rise analysis measurement methods. This information is passed over to the
 406 Burnvel routine that analyses the pressure rise data, so that data affected by the occurrence of
 407 cellularity can be excluded from the analysis

408

409 4.2 Pressure rise method

410 Following the initial flame propagation, as the unburned gas ahead of the flame front is compressed
 411 the adiabatic core undergoes isentropic compression, thereby increasing the temperature and pressure
 412 into which the flame front is propagating.

413

414 The pressure rise is measured at a sample rate of 10 kHz, and at each point the burning velocity is
 415 calculated using the equation for burning velocity of Lewis and von Elbe [12], combined with the
 416 multizone combustion model of Saeed and Stone [20] to avoid the inaccuracies encountered with the
 417 Lewis and von Elbe assumption of a linear relationship between the mass fraction burned and
 418 pressure rise. Burning velocity is calculated from:

$$S_u = \frac{dr_i}{dt} \left(\frac{r_i}{r_b} \right)^2 \left(\frac{p_i}{p} \right)^{\frac{1}{\gamma_u}} \quad (6)$$

419 which is obtained from considering the volume of an elemental shell of unburned gas at the time of
 420 burning, e.g. [52]. The radius of that elemental shell before any burning takes place is r_i , and by the
 421 time it burns, has been compressed such that it has radius r_b , where p_i is the initial pressure, and γ_u is
 422 the ratio of specific heats of the unburned gas. The radius of the shell corresponding to a given mass
 423 fraction burned, x , before any combustion takes place is found from:

$$r_i = \sqrt[3]{xR^3} \quad (7)$$

424 where R is the radius of the vessel. To determine x at a particular point in combustion, the multizone
 425 model is used to relate x to p . This is implemented as the BOMB program shown on the schematic
 426 diagram in Fig. 4. The flame radius, r_b is also found from the BOMB program along with the
 427 unburned gas temperature, the ratio of specific heats of the unburned gas (γ_u) and the burned gas
 428 temperature distribution. The outputs from the bomb program are then passed to the Burnvel routine,
 429 where they are used to calculate burning velocity for each of the values of pressure recorded during
 430 the experiment (as seen in Fig. 4a, which also shows the fit of the a polynomial to the data selected
 431 from this experiment for the correlation). The range of data to be included in the overall data set for
 432 the correlation is selected to ensure that only data at valid conditions is used. This involves removal
 433 of the initial early burn period, where the small pressure rise is subject to noise, and the end of the
 434 pressure rise, where heat transfer to the vessel wall becomes significant resulting in inaccurate values

of the burning velocity being determined. In addition, any detection of cellularity (as occurred in Fig 4a) will require the data range to be reduced to exclude any cellular data from the data set. The selected data is shown in Fig. 4b, along with the output from the subsequent correlation that comes from the fit to all of the experiments.

The data selection process is repeated for each experiment in the experimental set, over the range of equivalence ratios, diluent fractions and initial temperatures and pressures of interest. The data points from each experiment (the number of which will depend upon the duration of combustion and the presence of any flame front instabilities) are compiled into a single data set. A correlation fitting routine, fitcorr, is used to fit a 14 term correlation to the data, to represent the effects of equivalence ratio, temperature, pressure and diluent fraction. The 14 term correlation is based upon that of Marshall [23], but with a second order dependence on equivalence ratio included in the temperature and pressure exponents following the findings of Konnov *et al.* [47], as given in equation (8):

$$S_u = [S_{u,0} + S_{u,1}(\phi - 1) + S_{u,2}(\phi - 1)^2 + S_{u,3}(\phi - 1)^3 + S_{u,4}(\phi - 1)^4] \quad (8)$$

$$\times T^\varepsilon \times P^\beta \times \left(1 - \mu_1 x_r^{(\mu_2 + (\phi - 1)\mu_3)}\right)$$

Where:

$$\varepsilon = \varepsilon_0 + \varepsilon_1(\phi - 1) + \varepsilon_2(\phi - 1)^2$$

$$\beta = \beta_0 + \beta_1(\phi - 1) + \beta_2(\phi - 1)^2$$

$$T = \frac{T_u}{298} ; P = \frac{P_u}{1.0}$$

The fitcorr algorithm fits the data to the correlation by using a least squares minimisation routine. As a check of the quality of fit, the correlation is plotted against the data from each experiment in turn, e.g. Fig. 4b . The determined coefficients can then be evaluated for any desired conditions, e.g. Fig. 4c.

A difficulty encountered in the correlation fitting procedure is one of uneven data spread across the range of equivalence ratios and conditions tested. The biggest cause of this is the onset of cellularity which limits the pressure to which data can be included. The pressure at which this onset occurs differs depending on the mixture composition, meaning that for a test sequence involving a range of equivalence ratios, there will be a skew of data towards one end of the data set. It is important to ensure that burning velocity correlations are used only for the conditions over which tests have been performed. For example, many values of burning velocity in the literature are reported for ambient conditions of temperature and pressure, but given that the pressure must rise to use this technique, data at these conditions will not have been included in the fitting.

4.3 Sources of Error

The sources of error can be separated into three parts: those associated with mixture preparation, combustion measurements and data analysis.

For mixture preparation the fill pressure was always just over 4 bar, even when a much lower pressure was needed, since this enabled the 6 bar Druck PMP1400 piezo-resistive pressure

transducer to be used at the top of the range over which it had been calibrated (0 to 4.5 bar). The transducer had a combined non-linearity, hysteresis and repeatability error of below 0.15%. The final fill pressure can be considered to be accurate to $\pm 0.2\%$. When using gaseous fuels an appropriate transducer was used and the accuracy was in the range $\pm 0.2 - 0.5\%$, (allowing for the different partial pressure of fuels and diluents). The liquid fuel injection required measurement of the syringe and needle mass before and after injection. The balance had a resolution 0.1 mg and with a minimum of 300 mg injected, then errors here can be ignored. Since injection was with the vessel below atmospheric pressure there were no concerns about fuel not entering the vessel. Calculation of the number of moles also requires an absolute temperature measurement, and the type K thermocouple system had an accuracy of $\pm 0.7\text{ K}$ or $\pm 0.2\%$. It is also possible that the thermocouple did not record the gas temperature correctly, but this was monitored during the 5 minute settling period between the end of mixture preparation and ignition. This also provided the opportunity to monitor leaks, so an acceptable fall in pressure can be linked to a loss of mixture during the fill process, such that the error in λ was no more than $+0.1\%$. If all of the errors were to combine in the worst way the error in mixture preparation would be $+1.0$ to -0.9% . Since the effect of errors (other than those associated with leakage) will be random, an rms approach can be used on these errors to give a likely error range in mixture preparation of $+0.5$ to -0.4% . These errors apply to individual experiments and are thus directly relevant to burning velocity measurements derived from the flame front imaging. When data from pressure rise data is combined from multiple experiments, then the effect of random errors will be greatly reduced (by a factor proportional to the square root of the number of experiments). A Fortin barometer was used for measuring atmospheric pressure so the greatest error here would be from changes in pressure during the course of a morning or afternoon, but even a change of 5 mbar would in fact be negligible.

The second type of error concerns measurements during combustion, and for flame speed imaging the key factor is the 512×512 pixel resolution of the camera. Image scaling is from the window aperture of $40 \pm 0.1\text{ mm}$, and the flame velocity will determine the accuracy. With a typical speed of 2 m/s and a frame rate of 3000 pps, this corresponds to a radius increase of 0.66 mm/frame (or 17 pixels on diameter/frame), so with two measurements of diameter this corresponds to an error of 4%, but since a straight-line is fitted to a dozen or so such measurements the error is reduced to about 0.3%. The third type of error is associated with data analysis, and as explained in Section 2 there are errors associated with the line-fitting extrapolation that are influenced by the selection of the data points (an example will be seen later in Fig. 4d). Such errors are very difficult to quantify but experiments with different fits suggest errors are below 3%, and this is the most significant source of error when flame speed measurements are being used.

For burning velocity measurements derived during the pressure rise phase the second type of error arises from the calibration of the transducer. The transducer and amplifier were calibrated as a pair, and for the 0-40 bar pressure range the maximum error was 0.1 bar using a linear fit, but this was reduced to below 0.04 bar (0.1% of fsd) by using a parabolic fit. Separate calibrations with higher gains were used for the 0-8 and 0-16 bar pressure ranges. With a 12 bit DAQ card digitisation errors are negligible. Data analysis errors (type 3 errors) are more complex. Numerical modelling shows that to a first order a 1% error in pressure measurement will lead to a 1% error in the computed burning velocity (the fractional pressure rise is not quite proportional to the mass fraction burned). The data analysis requires differentiation and the noise in real data is 'amplified' by this process (as seen in Fig. 2), but the subsequent polynomial fitting acts as a filter. The data selected for analysis usually starts once the pressure has risen by about 50%, by which time differentiation noise is much reduced (this can be seen in Fig 4b). It is essential that data affected by cellularity is discarded and the schlieren system detects this before there is any noticeable deviation in the computed burning velocity data. Errors can also be introduced by fitting a correlation of the wrong form to the data,

and since the correct form of the correlation is unknown, then this possible error cannot be quantified. That said, the fit of the correlation is checked to each experiment (as seen in Fig 4b), and this has failed to identify any systematic error trends. Further reassurance that the correlation fits the data is provided later when results are compared between the two independent methods.

5 Results

A comparison of the two techniques is demonstrated here using results from tests with methane-air, methane-air-carbon dioxide and ethanol-air mixtures at a range of temperatures and pressures. The methane was commercially pure, and the biogas was 60% methane and 40% carbon dioxide by volume. The ethanol was 99.5% pure and taken from a 2.5 L bottle that was sealed when not in use, so as to minimise absorption of water vapour.

Firstly, the range of data obtained from the tests is discussed, followed by the results of the correlation fitting, and finally a comparison of the two techniques. Tests were performed on the mixtures using both methods, over a range of equivalence ratios that ranged from 0.7 to 1.4, initial temperatures of 380 K and 450 K, and pressures 0.5, 1, 2 and 4 bar. Note however, that few tests were performed at 0.5 bar due to difficulties in igniting these mixtures away from stoichiometric. The total number of tests performed was about 60 for each fuel, resulting in about 50000 data points for each fuel. The range of data included in the data set to which the correlation is fitted is presented in Table 1; Table 1 shows the maximum and minimum values of various parameters. However, the data is not spread evenly across the range of equivalence ratio and pressure. For example, with ethanol the data is skewed towards lean mixtures as a result of the earlier onset of cellularity in rich mixtures, and this limited the range of high pressure data obtained.

Table 1– Maximum and minimum values in the ethanol, methane and 60% methane/40% carbon dioxide (60/40 biogas) data sets

| Property | Ethanol | | Methane | | 60/40 Biogas | |
|---------------|---------|------|---------|------|--------------|------|
| | Min | Max | Min | Max | Min | Max |
| T_0 (K) | 380 | 450 | 380 | 450 | 298 | 450 |
| P_0 (barA) | 0.5 | 4.0 | 0.5 | 4.0 | 1.0 | 4.0 |
| Φ | 0.70 | 1.40 | 0.70 | 1.40 | 0.70 | 1.20 |
| P_u (barA) | 0.66 | 16.9 | 0.64 | 16.4 | 1.23 | 12.1 |
| T_u (K) | 393 | 633 | 394 | 652 | 349 | 648 |
| S_u (cm/s) | 21.9 | 106 | 15.6 | 106 | 15.6 | 68.3 |
| S_f (cm/s) | 40.5 | 351 | 25.1 | 351 | 27.1 | 183 |
| α (/s) | 10.8 | 146 | 7.1 | 148 | 7.1 | 78 |
| r_b (mm) | 39.4 | 77.4 | 37.3 | 77.5 | 44.5 | 77.4 |
| t (ms) | 14.5 | 92.3 | 16.1 | 159 | 25.4 | 123 |

Correlations of the form of equation (8) were fitted to the data, and the correlation coefficients are summarised in Table 2.

Table 2 – correlation coefficients for ethanol, methane and 60% methane/40% carbon dioxide (60/40 biogas) data sets

| | $S_{u,0}$ | $S_{u,1}$ | $S_{u,2}$ | $S_{u,3}$ | $S_{u,4}$ | ε_0 | ε_1 | ε_2 | β_0 | β_1 | β_2 |
|--------------|------------------|-----------|------------------|-----------|--------------------|-----------------|--|-----------------|-----------|-----------|-----------|
| Ethanol | 35.616 | 21.159 | -130.38 | -38.952 | 79.839 | 1.9195 | -0.2463 | 2.3624 | -0.2596 | 0.2100 | -0.3089 |
| Methane | 30.799 | 1.6141 | -241.19 | -22.214 | 680.84 | 2.0879 | 0.17135 | 5.4338 | -0.3463 | -0.0419 | -0.9067 |
| 60/40 Biogas | $\mu_1 = 1.1050$ | | $\mu_2 = 1.1779$ | | $\mu_3 = -0.76207$ | | As defined in equation 8, with $x = 0.4$ | | | | |

These correlations are compared with the results of the image analysis in Figure 5 for ethanol, in Fig. 6 for methane, and in Fig. 7 for biogas (represented here by 60% methane/40% carbon dioxide). These figures all show a good agreement between the results from the two methods: the correlations and the results from the flame front imaging analysis. The agreement is mostly well within the accuracy of the measurements, especially when it is noted that when the initial temperature is 380 K, then evaluating the correlation at 380 K required a slight downward extrapolation.

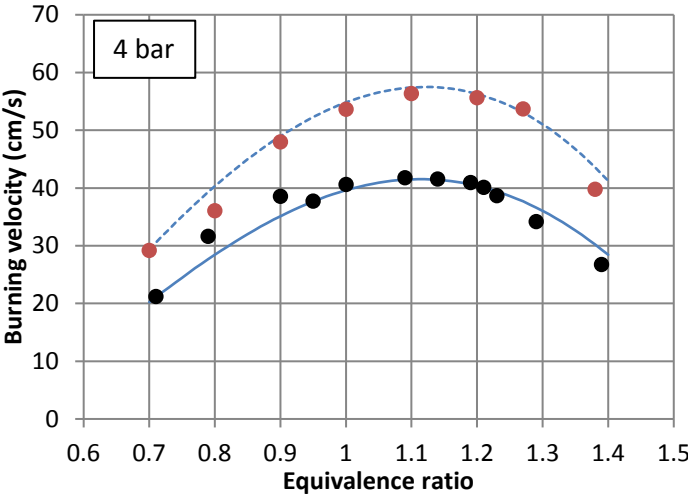
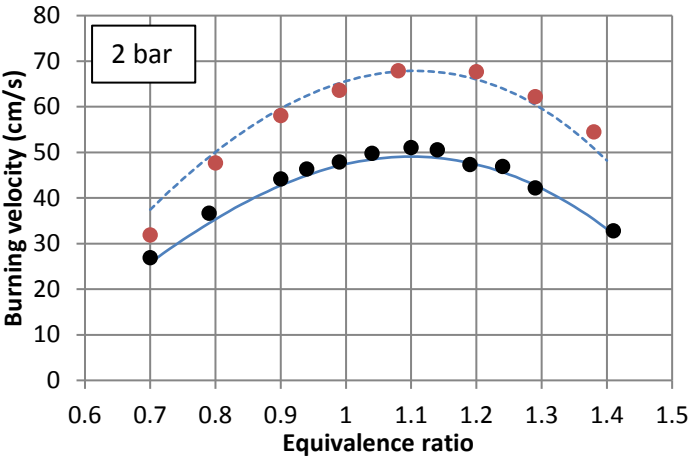


Figure 5 – Ethanol-air burning velocity results at 2 bar and 4 bar. Lines represent the results from the correlation (defined in Eq. 8 with coefficients from Table 2) at 380 K (solid line) and 450 K (dashed line); points represent results from schlieren image analysis.

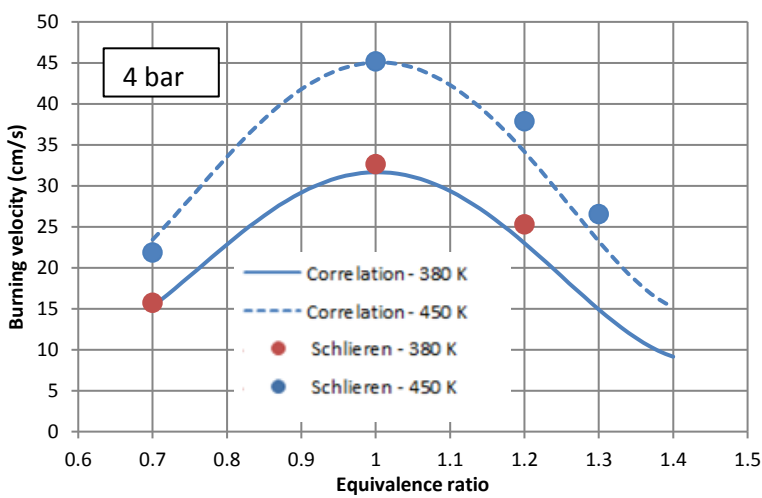
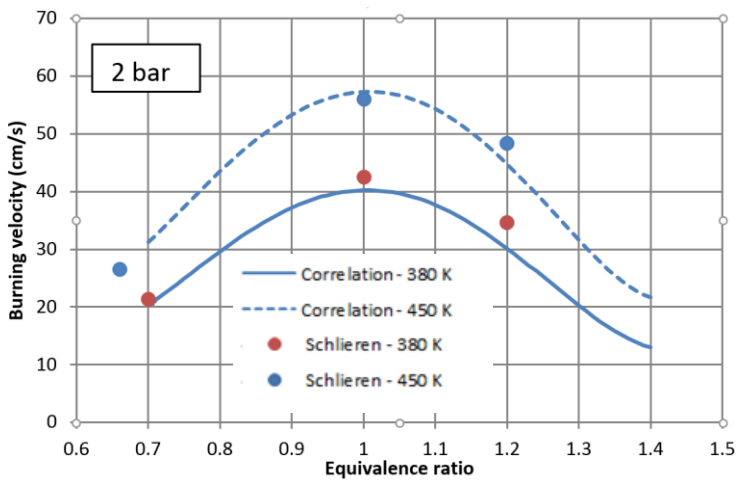
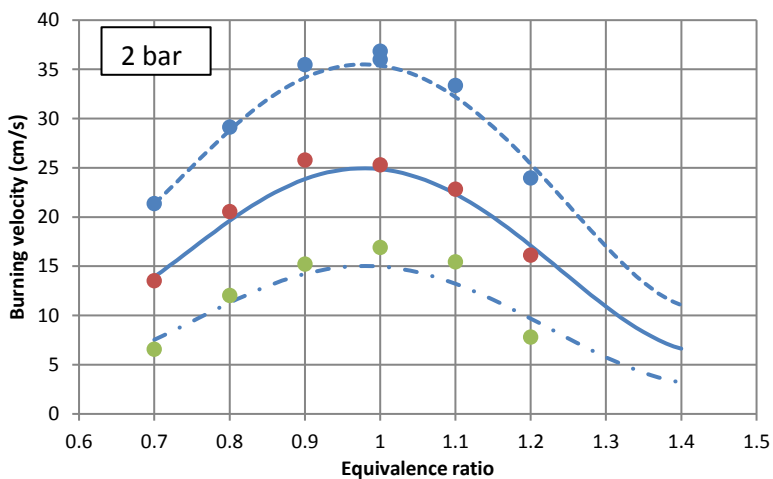


Figure 6 – Methane-air burning velocity results at 2 bar and 4 bar. Lines represent the results from the correlation (defined in Eq. 8 with coefficients from Table 2) at 380 K (solid line) and 450 K (dashed line); points represent results from schlieren image analysis.



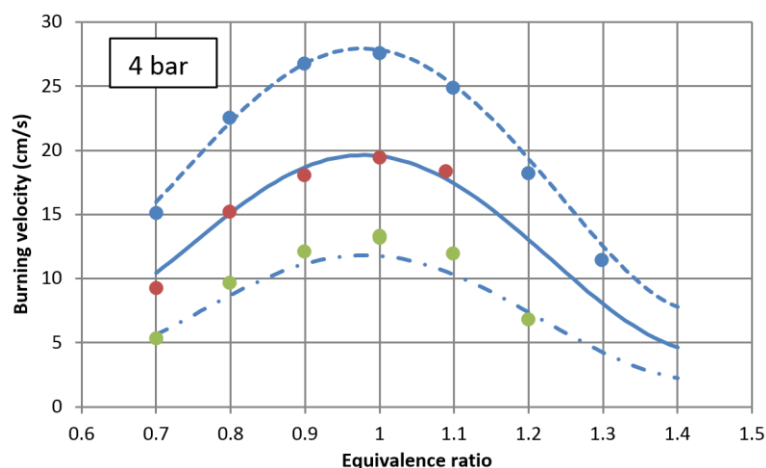


Figure 7 – Biogas (represented here by 60% methane and 40% carbon dioxide by volume) - air burning velocity results at 2 bar and 4 bar. Lines represent the results from the correlation (defined in Eq. 8 with coefficients from Table 2) at 298 K (chained line) 380 K (solid line) and 450 K (dashed line); points represent results from schlieren image analysis.

Comparisons with published data are very difficult, since the data presented here are for elevated pressures and temperatures. Figure 8 shows a comparison for stoichiometric methane, though the correlation has required extrapolation down to 298 K and additional extrapolation when pressures are below about 1.5 bar.

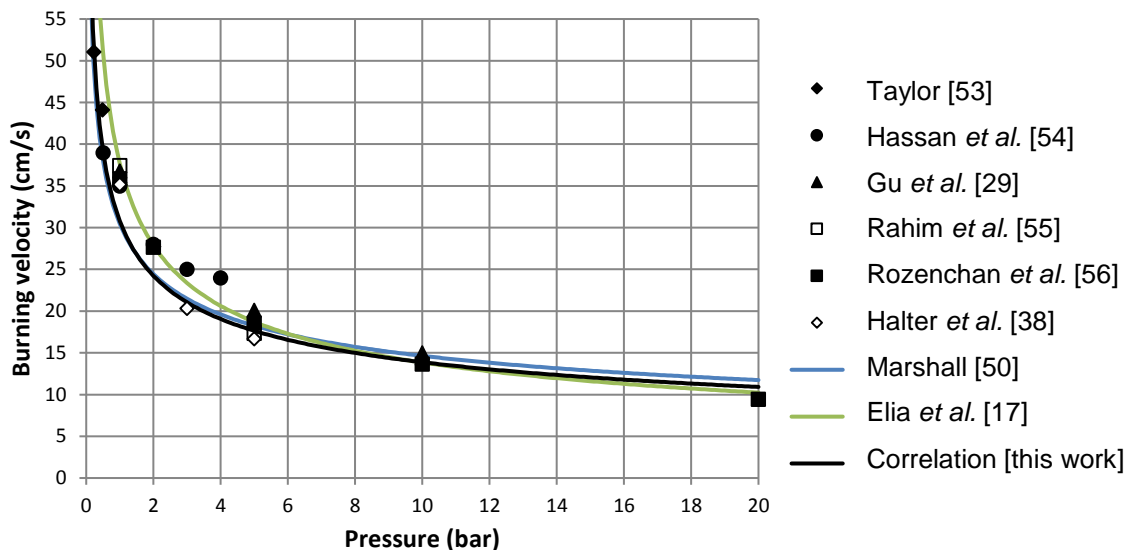


Figure 8 – Stoichiometric methane-air correlations at 298 K, varying pressure, compared with results from the literature – it should be noted that the correlation has required extrapolation down to 298 K.

For ethanol comparable data was not found, but some comparisons are shown in Figure 9, but these required downwards extrapolation of both the temperature and pressure for the correlation. Agreement is good for weak mixtures but poor when rich of stoichiometric; this coincides with a more limited set of high pressure data because of the onset of cellularity.

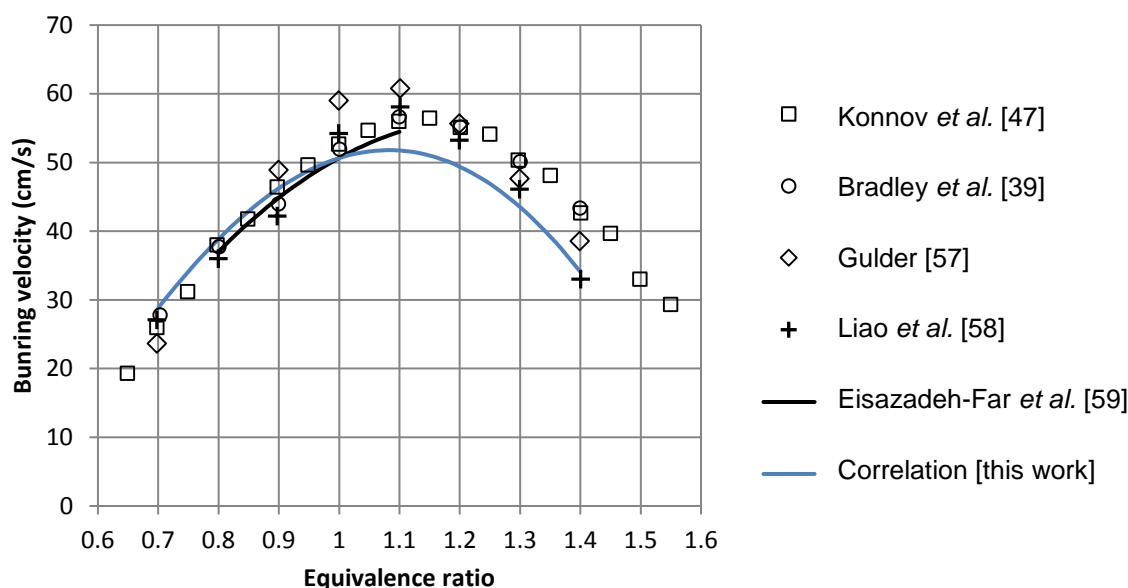


Figure 9 – Comparison of the correlation for ethanol with literature values at 1 bar and 358 K; note that this has required downwards extrapolation of both the temperature and pressure for the correlation.

6 Conclusions

The values of the burning velocity that have been presented here for mixtures of air with ethanol, methane and biogas (60% methane and 40% carbon dioxide by volume) are for elevated temperatures and pressures so there is very little published data for comparison. Where data exists the comparisons are satisfactory, and when the correlations are extrapolated to lower temperatures and pressures the results are reassuring.

However, the focus of this paper is to show that with appropriate processing of the data from constant volume combustion vessels, it is possible to obtain consistent values of the laminar burning velocity using both flame front imaging and pressure rise data measurement methods. The flame front imaging corresponds to less than 1% of the fuel being burned, so the pressure rise is negligible. However, the small radii and high flame speeds mean that stretch has to be accounted for, so as to yield values of the un-stretched laminar burning velocity. With the pressure rise data, a combustion model is needed to calculate the flame front position from the pressure measurement and the state of the unburned gas. It is also essential to image the flame front, since if cellularity occurs, then the assumption of a smooth spherical flame is invalid. At least 10% of the fuel needs to be burned before the pressure-rise data can be used (as when the rate of pressure rise is small the differentiation within the analysis generates noise), by which time the effects of stretch are becoming negligible. It is also essential to exclude data affected by cellularity. Thus with suitable precautions and data analysis, then the two constant volume combustion techniques for laminar burning velocity measurements give consistent data.

Acknowledgement

Support from EPSRC EP/H031197/1 and Shell Global Solutions is gratefully acknowledged.

1. J. Vancoillie, J. Demuynck, J. Galle, S. Verhelst, A laminar burning velocity and flame thickness correlation for ethanol–air mixtures valid at spark-ignition engine conditions, *Fuel* 102 (2012): 460-469.
2. M. Baloo, B.M. Dariani, M. Akhlaghi, M. AghaMirsalim, Effects of pressure and temperature on laminar burning velocity and flame instability of iso-octane/methane fuel blend. *Fuel* 170 (2016) 235-244.
3. D. Bradley, M. Lawes, R. Mumby, Burning velocity and Markstein length blending laws for methane/air and hydrogen/air blends, *Fuel* 187 (2017) 268-275.
4. T. Badawy, J. Williamson, H. Xu, Laminar burning characteristics of ethyl propionate, ethyl butyrate, ethyl acetate, gasoline and ethanol fuels, *Fuel* 183 (2016): 627-640.
5. C.J. Rallis, A.M. Garforth, The Determination of Laminar Burning Velocity, *Prog. Energy Combust. Sci.* 6 (1980) 303-329.
6. K.J Bosschaart, L.P.H. de Goey, Detailed analysis of the heat flux method for measuring burning velocities, *Combust. Flame* 132 (2003) 170-180.
7. A.M. Katoch, A.S. Minaev, S. Kumar, Measurement of laminar burning velocities of methanol–air mixtures at elevated temperatures, *Fuel* 182 (2016) 57-63
8. M. Goswami, S.C.R. Derks, K. Coumans, W.J. Slikker, M.H. de Andrade Oliveira, R. J.M. Bastiaans, C.C.M. Luijten, L.P.H. de Goey, A.A. Konnov, The effect of elevated pressures on the laminar burning velocity of methane + air mixtures, *Combust. Flame* 160 (2013): 1627-1635.
9. B. Hopkinson, Explosions of Coal and Gas and Air. *Philos. Trans. R. Soc. London, Ser. A* 77 (1906) 387-413.
10. F.W. Stevens, The rate of flame propagation in gaseous explosive reactions. *J. Am. Chem. Soc.* 48 (1926) 1896-1906.
11. E.F. Fiock, C.F. Marvin Jr, F.R. Caldwell, C.H. Roeder, Flame speeds and energy considerations for explosions in a spherical bomb, *Natl. Advisory Comm. Aeronaut., Rep.*, 1940.
12. B. Lewis, G. von Elbe, *Combustion, Flames and Explosions of Gases* Academic Press Inc. London, UK 1961.
13. M. Metghalchi, J.C. Keck, Laminar Burning Velocity of Propane-Air Mixtures and High Temperature and Pressure, *Combust. Flame* 38 (1980) 143-145.
14. R. Stone, A. Clarke, P. Beckwith, Correlations for the Laminar-Burning Velocity of Methane-Diluent-Air Mixtures Obtained in Free-Fall Experiments, *Combust. Flame* 114 (1998) 546-555.
15. D. Bradley, A. Mitcheson, Mathematical Solutions for Explosions in Spherical Vessels, *Combust. Flame* 26 (1976) 201-217.
16. P.G. Hill, J. Hung, Laminar burning velocities of stoichiometric mixtures of methane with propane and ethane additives, *Combust. Sci. Tech.* 60 (1988) 7-30.
17. M. Elia, M. Ulinski, M. Metghalchi, Laminar Burning Velocity of Methane–Air–Diluent Mixtures. *J. Eng. Gas Turbines & Power* 123 (2001) 190.
18. W. Reynolds The element potential method for chemical equilibrium analysis: Implementation in the interactive program STANJAN, version 3. Technical Rept. 1986.
19. American Chemical Institute, A.I.o.P., National Bureau of Standards, JANAF Thermochemical Tables, 1986.
20. K. Saeed, C.R. Stone, The modelling of premixed laminar combustion in a closed vessel *Combust. Theory Modelling*, 8 (2004) 721-743.
21. C.R. Ferguson, *Internal combustion engines*, **p168-80** Wiley, New York 1985.
22. R.R. Raine, C.R. Stone, J. Gould, Modelling of Nitric Oxide Formation in Spark Ignition Engines with a Multi-zone Burned Gas, *Combust. Flame* 102 (1995) 241-255.

- 679 23. S.P. Marshall, S. Taylor, C.R. Stone, T.J. Davies, R.F. Cracknell, Laminar burning velocity
680 measurements of liquid fuels at elevated pressures and temperatures with combustion
681 residuals, *Combust. Flame* 158 (2011) 1920-1932.
- 682 24. B. Karlovitz, D.W. Denniston, D.H. Knapschaefer, F.E. Wells, Studies on Turbulent flames,
683 *Symp. (Int.) Combust.* 4 (1953) 613-620
- 684 25. A. Palm-Leis, R.A. Strehlow, On the propagation of turbulent flames, *Combust. Flame* 13
685 (1969) 111-129.
- 686 26. D. Bradley, R.A. Hicks, M. Lawes, C.G.W. Sheppard, R. Woolley, The measurement of
687 laminar burning velocities and Markstein numbers for iso-octane–air and iso-octane–n-
688 heptane–air mixtures at elevated temperatures and pressures in an explosion bomb, *Combust.*
689 *Flame* 115 (1998) 126-144.
- 690 27. G.E. Andrews, D. Bradley, Determination of burning velocities A critical review., *Combust.*
691 *Flame* 19 (1972) 275-288.
- 692 28. Z. Chen, M.P. Burke, Y. Ju, Effects of compression and stretch on the determination of
693 laminar flame speeds using propagating spherical flames, *Combust. Theory Modelling* 13,
694 (2009) 343-364.
- 695 29. X.J. Gu, M.Z. Haq, M. Lawes, R. Woolley, Laminar burning velocity and Markstein lengths
696 of methane–air mixtures, *Combust. Flame* 121 (2000) 41-58.
- 697 30. G. Markstein, Cell structure of propane flames burning in tubes, *J. Chem. Phys.* 17 (1949)
698 428-429.
- 699 31. J. Manton, G. Von Elbe, B. Lewis, Nonisotropic propagation of combustion waves in
700 explosive gas mixtures and the development of cellular flames. *J. Chem. Phys.* 20(1952) 153-
701 157.
- 702 32. A.S. Al-Shahrany, D. Bradley, M. Lawes, K. Liu, R. Woolley, Darrieus–Landau and thermo-
703 acoustic instabilities in closed vessel explosions, *Combust. Sci. Tech.* 178 , (2006) 1771-
704 1802.
- 705 33. D. Bradley, P.H. Gaskell, X.J. Gu, Burning Velocities, Markstein Lengths and Flame
706 Quenching for Spherical Methane-Air Flames A Computational Study. *Combust. Flame* 104
707 (1996) 176-198.
- 708 34. D.R. Dowdy, D.B. Smith, S.C. Taylor, The use of expanding spherical flames to determine
709 burning velocities and stretch effects in hydrogen-air mixtures. *Symp. (Int.) Combust.* 23
710 (1990).
- 711 35. A.P. Kelley, C.K. Law, Nonlinear Effects in the Experimental Determination of Laminar
712 Flame Properties from Stretched Flames, Eastern State Fall Technical Meeting - Physical and
713 Chemical Processes in Combustion 2007: University of Virginia.
- 714 36. Z. Chen, On the extraction of laminar flame speed and Markstein length from outwardly
715 propagating spherical flames, *Combust. Flame*, 158(2011) 291-300.
- 716 37. T. Tahtouh, F. Halter, C. Mounaïm-Rousselle, Measurement of laminar burning speeds and
717 Markstein lengths using a novel methodology, *Combust. Flame*, 156 (2009) 1735-1743.
- 718 38. F. Halter, T. Tahtouh, C. Mounaïm-Rousselle, Nonlinear effects of stretch on the flame front
719 propagation, *Combust. Flame*, 157(2010) 1825-1832.
- 720 39. D. Bradley, M. Lawes, M.S. Mansour, Explosion bomb measurements of ethanol–air laminar
721 gaseous flame characteristics at pressures up to 1.4MPa, *Combust. Flame*, 156 (2009) 1462-
722 1480.
- 723 40. C. Xiouris, T. Ye, J. Jayachandran, F.N. Egolfopoulos, Laminar flame speeds under engine-
724 relevant conditions: Uncertainty quantification and minimization in spherically expanding
725 flame experiments, *Combust. Flame* 163 (2016) 270–283.
- 726 41. E. Varea, V. Modica, A. Vandel, B. Renou. Measurement of laminar burning velocity and
727 Markstein length relative to fresh gases using a new postprocessing procedure: Application to

- laminar spherical flames for methane, ethanol and isooctane/air mixtures, *Combust. Flame* 159 (2012) 577-590.
42. E.G. Groff, The cellular nature of confined spherical propane-air flames, *Combust. Flame* 48(1982) 51-62.
 43. J.T. Farrell, R.J. Johnston, I.P. Androulakis, Molecular Structure Effects On Laminar Burning Velocities At Elevated Temperature And Pressure. SAE Technical Paper2004-01-2936, 2004.
 44. F Lindström, HE Angstrom, G Kalghatgi, CE Möller, An Empirical SI Combustion Model Using Laminar Burning Velocity Correlations, SAE Technical Paper, 2005-01-2106, 2005.
 45. M. Metghalchi, J.C. Keck, Burning Velocities of Mixtures of Air with Methanol, Isooctane and Indolene at High Pressures and Temperatures, *Combust. Flame*, 48 (1982) 191-210.
 46. G. Kalghatgi, *Fuel/Engine Interactions*: SAE International, 2014.
 47. A.A. Konnov, R.J. Meuwissen, L.P.H. de Goey, The temperature dependence of the laminar burning velocity of ethanol flames. *Proc. Combust. Inst.* 33 (2011) 1011-1019.
 48. S.P. Marshall, R. Stone, C. Hegheş, T.J. Davies, R.F. Cracknell, High pressure laminar burning velocity measurements and modelling of methane and n-butane, *Combust. Theory Modelling*, 14 (2010) 519-540.
 49. N. Hinton, R. Stone, Laminar burning velocity measurements of methane and carbon dioxide mixtures (biogas) over wide ranging temperatures and pressures. *Fuel* 116 (2014) 743-750.
 50. S. Marshall, *Measuring Laminar Burning Velocities*, DPhil Thesis in Department of Engineering Science 2010, University of Oxford.
 51. C.C.M. Luijten, L.P.H. De Goey, New, Accurate, Analytical Relations for Fractional Pressure Rise, Laminar Burning Velocity, and the Cubic Root Law in Constant Volume Combustion, *Proc. 3rd European Combustion Meeting* 2007.
 52. K. Saeed, C.R. Stone, Measurements of the laminar burning velocity for mixtures of methanol and air from a constant-volume vessel using a multizone model. *Combust. Flame*, 139 (2004) 152-166.
 53. S.C. Taylor, *Burning velocity and the influence of flame stretch*, PhD thesis, University of Leeds (1991).
 54. M.I. Hassan, K.T. Aung, G.M. Faeth, Measured and Predicted Properties of Laminar Premixed Methane-Air Flames at Various Pressures, *Combust. Flame* 115 (1998) 539-550.
 55. F. Rahim, M. Ulinski, M. Metghalchi, Burning velocity measurements of methane-oxygen-argon mixtures and an application to extend methane-air burning velocity measurements, *Int. J. Engine Res.* 3 (2002) 81-92.
 56. G. Rozenchan, D.L. Zhu, C.K. Law, S.D. Tse, Outward Propagation, Burning Velocities, and Chemical Effects of Methane Flames up to 60 atm, *Proc. Combust. Inst.* 29 (2002) 1461-1469.
 57. O.L. Gülder, Laminar burning velocities of methanol, ethanol and isooctane-air mixtures, *Symp. (Int.) Combust.* 19 (1982) 275-281.
 58. S. Y. Liao, D.M. Jiang, Z.H. Huang, K. Zeng, Q. Cheng, Determination of the laminar burning velocities for mixtures of ethanol and air at elevated temperature, *Appl. Therm. Eng.* 27 (2007) 374-380.
 59. K. Eisazadeh-Far, A. Moghaddas, J. Al-Mulki, H. Metghalchi, Laminar burning speeds of ethanol/air/diluent mixtures, *Proc. Combust. Inst.* 33 (2011) 1021-1027.